Band Gap Reduction and Petal-like Nanostructure Formation in Heavily Ce-doped ZnO Nanopowders

Kamakhya Prakash Misra[1], Ashok Kumawat[1], Priyanka Kumari[2], Susruta Samanta[2], Nilanjan Halder[1], Saikat Chattopadhyay[1,*]

[1] *Department of Physics, School of Basic Sciences, Manipal University Jaipur, Jaipur, Rajasthan 303007, India*
[2] *Department of Chemistry, School of Basic Sciences, Manipal University Jaipur, Jaipur, Rajasthan 303007, India*

The objective of the present study is to explore the structural and optical behavior of a heavily Ce-doped ZnO nanoparticle system. Well-known chemical sol-gel method is adopted for the synthesis of the nanoparticles and its structural, optical, and morphological features are characterized. XRD and EDX analysis verify the presence of Ce atom in prepared sample. XRD data confirm that the Ce^{3+} ions occupy the Zn^{2+} ion sites in the hexagonal ZnO lattice during doping process. Due to higher doping concentration, excess Ce shows the presence of mixed CeO_2 and Ce_2O_3 phases in the sample. W-H analysis helps to understand the micro-strain profile in the grown sample. UV-Vis study confirms the band gap shifting in doped samples and Photoluminescence study gives the indication of the presence of defect states which are the reason behind NBE transitions in the samples. Prepared sample were also characterized using FESEM to analyze the surface morphology and nanocrystalline structures.

Keywords: ZnO, Rare earth material, Doping, Nanoparticles, Band gap, Photoluminescence.

1. INTRODUCTION

The design, synthesis, and use of nanosized materials are one of the important innovations in the last two decades, which found an extensive range of applications in numerous fields including medicine, engineering, technology, catalysis, and environmental remediation. Zinc oxide (ZnO) is one of the most interesting materials from several points of view and the attention in ZnO is fueled up due to its well-known distinctive properties, viz, high-sensitivity, large specific area, non-toxicity, good photocatalytic activity and a high isoelectric point, which all favor it to be considered as one of the most suitable II-VI semiconductor materials. Due to its wide band gap (~ 3.37 eV at room temperature) and large excitonic binding energy (60 meV), some optoelectronic applications of ZnO overlap with that of GaN, another wide band gap material popularly used in semiconductor industry to generate green, blue ultraviolet, and white light-emitting devices. Based on its simple, low cost, and easy process of synthesis ZnO becomes a more potential candidate to replace GaN to design modern semiconductor devices [1-5]. To design ZnO based nanodevices, one of the most relevant issues is introducing foreign element into pure ZnO as dopant. Extensive research has been conducted on the electronic and magnetic properties of the ZnO nanoparticles (NPs) or thin films doped with foreign atoms for nanoelectronic and spintronic device applications. The results satisfactorily show that electronic and magnetic properties of ZnO nanosystems can be modified by such kind of doping [2, 6-11]. Particularly, doping with optically functional impurities like transition metals (TM) or rare earth (RE) elements permits the extension of the emission wavelength range from visible to the in-frared region. Multi-wavelength and white light emission becomes possible from a single nanodevice by choosing a combination of several suitable dopants or co-dopants [7]. Nowadays the RE elements are more interesting materials as a dopant for ZnO as 4*f* shell of RE elements shows larger magnetic moments and the electrons may intervene the ferromagnetic coupling between the RE ions due to the coupling between *f* electrons and host *s* electrons which makes such systems more suitable to design both optoelectronic and spintronic devices [7, 12].

According to Jayachandraiah et al. [12] among all other RE elements, in the recent past, Cerium (Ce) has received much more attention due to its strange optical, luminescence, magnetic, and catalytic properties arising from the availability of the shielded 4*f* levels with only one electron in the 4*f* state. Although a rigorous study on optical properties of Ce-ZnO nanosystems have been started but still the origin of optoelectronic and magnetic properties is remains unsolved. This motivated us to investigate the influence of Ce doping in ZnO NPs to understand the optical and electronic properties in a systematic way to conclude its use in preparing modern nanodevices.

Hence, the objective of the present work is to study, the structural and electronic properties of Ce-doped ZnO NPs synthesized through a simple cost-effective chemical sol-gel route. The synthesized heavily doped (Ce, 10 at. %) sample will be denoted as CZO in present discussion. The synthesized sample was then investigated using X-ray diffraction (XRD) method to understand its structural properties. To study the optical and electronic properties, we use UV-Vis and Photoluminescence (PL) method and finally to analyze the micro-

structural properties FESEM images were captured with different magnification range. EDX helps to identify the elements present in the prepared sample. Finally, an attempt has been made to correlate the structural and optical observations to discuss its utility to design modern light emitting or sensor devices.

2. EXPERIMENTAL DETAILS

2.1 Material Synthesis

Undoped ZnO and Ce-doped $Zn_{1-x}Ce_xO$ (where $x = 0$ and 0.1) NPs were synthesized through chemical co-precipitation method. It is very popular and widely used technique to prepare NPs due to its ease of processing and cost effectiveness. The details of the method can be found in our previous report [4, 5]. A complete flow chart, to understand the adopted chemical synthesis process easily, is given in Fig. 1.
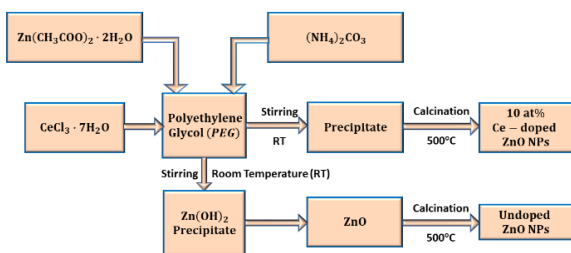

Fig. 1 – Flow chart of the chemical synthesis process of Ce doped ZnO NPs

2.2 Characterization Techniques

To study the structural properties of our prepared powder sample, after a proper heat treatment (500 °C) in oxygen environment for 3 h, we used X-ray diffraction method (Make: PAN analytical Empyrean, Model) with CuK$_\alpha$ radiation of wavelength 1.5418 Å having Cu anode and Ni filter following Bragg-Brentano geometry in the wide-angle (2θ) region from 25° to 85°. One can find a complete analysis of our undoped ZnO sample in our previous report [4, 5]. The Williamson-Hall (W-H) plots were obtained from the XRD data to determine particle size and the impact of micro-strain on peak broadening.

The FTIR spectroscopy was used to identify the various functional groups present in the samples with a typical Fourier transform infrared spectrometer (Make: Alpha, Bruker, Germany) within a range of 4000-500 cm^{-1}. The UV-Vis spectroscopy of all the samples was carried out using a standard UV-Vis equipment (Make: Shimadzu UV2600, Japan) after dispersing them in ethanol solution followed by sonication for 30 min. The spectra were recorded in transmission mode within the wavelength range of 200 to 600 nm. To study the optical properties, photoluminescence (PL) emission spectra of the sample were recorded using a standard photoluminescence spectrometer (Make: Horiba Fluoromax 4c, Horiba, USA) with an excitation wavelength of 310 nm and 325 nm. The morphology of sample was observed using field emission scanning electron microscope (FESEM) (Make: JEOL-7610F, Japan). For elemental analysis of the sample, energy dispersive X-ray (EDX) method is adopted.

3. RESULTS AND DISCUSSION

3.1 X-ray Diffraction

The XRD pattern and its complete analysis of un-doped ZnO NPs is already reported in our previous publication [4, 5]. The XRD pattern of CZO is shown in Fig. 2a. It clearly confirms the hexagonal wurtzite structure with observed prominent crystal peaks like (100), (002), (101), (102), (110), (103), (200), (112), (201), (004) and (202). Here, it is worthy to note that a weak signal corresponding to the crystal plane (111) of cubic CeO_2 can be observed at the position $2\theta = 28.64°$ which indicates the possibility of partial oxidation of Ce^{3+} into Ce^{4+} during the high temperature (500°) annealing process which leads to the formation of CeO_2. Major peak positions and interplanar spacing collected from XRD data are listed in Table 1. Doping causes a shift in peak positions towards lower 2θ angle. It may be a result of the local strain generated due to the doping of Ce^{3+}. It is well-known that Ce^{3+} have, comparatively a larger ionic radius (0.103 nm) than Zn^{2+} (0.074 nm) [13] and the strain is generated in the NPs when it is replacing Zn^{2+} ions in ZnO host lattice to settle down to form a stable structure.
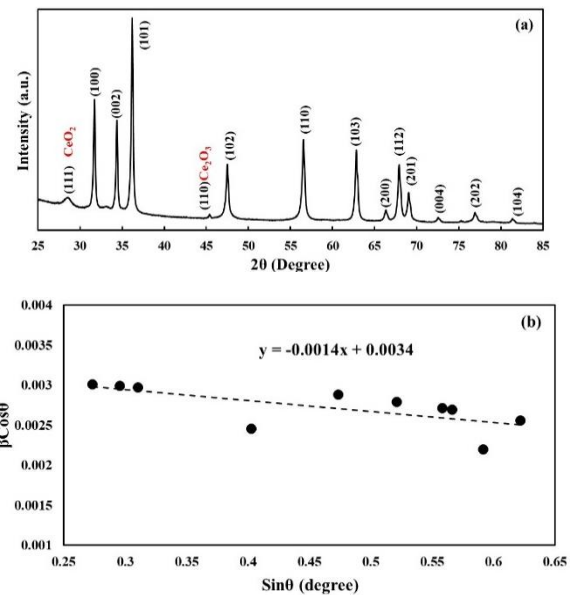

Fig. 2 – (a) XRD patterns of 10 at. % Ce doped ZnO NPs and (b) Williamson-Hall (W-H) plot of 10 at. % Ce-doped ZnO NPs

Table 1 – Positions and peak shift of major peaks after doping

Sample	Peaks		
	(100)	(002)	(101)
ZnO (2θ) [4, 5]	32.0831	34.7757	36.4580
CZO (2θ)	31.7340	34.3935	36.2172
dZnO (Å) [4, 5]	2.7876	2.5776	2.4625
dCZO (Å)	2.8198	2.7008	2.6076

The orientation parameters (γ_{hkl}) for CZO sample considering three prominent peaks (100), (002) and (101), have been calculated to understand the preferred growth orientation using the formula [14]:

Table 2 – Orientation parameter, crystallite size, dis-location density, strain, lattice parameters, u-value, volume, and bond length calculated from XRD data

	(100)	(002)	(101)
Orientation parameter (γ_{hkl})	0.2744	0.2277	0.4980
t_{DS} (nm)	46.15	46.47	46.75
Dislocation density (δ) ($\cdot 10^{14}$) (m^{-2})	4.695	4.631	4.576
t_{WH} (Å)	40.78		
Strain (ε)	$-0.07 \cdot 10^{-2}$		
d-spacing (Å)	2.8198	2.7008	2.6076
a (Å)	3.2560		
c (Å)	5.4016		
c/a	1.6589		
u-value	0.3711		
Volume (Å)^3	49.5917		
Bond length (Å)	2.0047		

$$\gamma_{hkl} = I_{hkl} / \sum I_{hkl}. \qquad (1)$$

Here, I_{hkl} represents the intensities of the corresponding crystallographic planes with Miller indices (hkl). Calculated γ_{hkl} values for CZO sample are listed in Table 2. The variation of the data indicates a random distribution of crystallographic planes in the sample. The lattice constants a and c are calculated using formula for wurtzite structure of ZnO [4, 14]

$$\frac{1}{d^2} = \frac{4}{3}\left(\frac{h^2 + hk + k^2}{a^2}\right) + \frac{l^2}{c^2}. \qquad (2)$$

Both the lattice constants (a and c) for CZO sample are larger than undoped ZnO [4] which is the indication of proper settlement of Ce^{3+} ions at interstitial sites of the ZnO host lattice. The Zn–O bond length is calculated in this case using the formula [4, 14]

$$L = \sqrt{\frac{a^2}{3} + \left(\frac{1}{2} - u\right)c^2}. \qquad (3)$$

Here,

$$u = \frac{1}{3}\left(\frac{a^2}{c^2}\right) + \frac{1}{4}. \qquad (4)$$

The particle sizes are calculated along different planes using the well-known Debye-Scherrer formula [4, 14]

$$t_{DS} = \frac{k\lambda}{\beta \cos\theta}, \qquad (5)$$

where β is the full width at half maximum (FWHM) of the given peak, θ is the corresponding angle of Bragg diffraction, λ is the wavelength of X-ray used (1.5406 Å) and k is a constant (value = 0.9). Calculated particle size (t_{DS}) along different planes is approximately 46 nm and tabulated in Table 2. The crystallite sizes confirm uniform nanocrystalline nature of the CZO samples along all the major planes. Calculated dislocation densities (δ_{hkl}) [4, 14] vary between $\sim 4.65 \cdot 10^{14}$ m^{-2} to $\sim 4.576 \cdot 10^{14}$ m^{-2} which is as expected. Based on the

experimental data, a W-H analysis is done to understand the strain profile using the equation [4, 14]

$$\beta \cos\theta = \frac{C\lambda}{t_{WH}} + 2\varepsilon \sin\theta. \qquad (6)$$

Here, t_{WH} is crystallite size, ε is strain, λ is the wavelength used and β is FWHM. The constant C is a correction factor, and it is taken as 1. A graph between $\beta\cos\theta$ and $\sin\theta$ is plotted in Fig. 2b for CZO which is obviously fitted very well as a straight line. From the slopes and intercepts of the linear fit equation, the magnitudes of t_{WH} and ε are determined. The negative sign indicates the microstrain is compressive in this case. As per our previous report, the microstrain calculated for undoped ZnO is $-5.19 \cdot 10^{-2}$ [4] which is too higher in comparison to the doped sample. They were simultaneously synthesized and further treated under the same conditions, which further support our claim that the Ce ions after doping settle down properly in the ZnO matrix, reducing the microstrain.

3.2 FTIR Analysis

The Fourier transform infrared (FTIR) spectrum was recorded to explore the chemical bonding of CZO sample. It was recorded between 500-4000 cm^{-1} in the transmission mode and the results are displayed in Fig. 3. As expected, the vibrational bands observed within 1000 cm^{-1} are influenced due to the inorganic elements. The presence of Ce ions in the CZO sample was clearly elucidated by the occurrence of a peak at 575 cm^{-1} [13] and the other infrared absorption bands observed at 678 cm^{-1} and 833 cm^{-1} are due to the Ce-O bonding [15]. The stretching modes of C–O and C=O were observed around 1396 cm^{-1} and 1524 cm^{-1} as shown in Fig. 3. [13, 15]. A dip at 2324 cm^{-1} is a signature of C–H groups [15]. No other major bands except those mentioned here are detected in the FTIR spectrum which substantiates that the synthesized nanoparticles are almost pure without any significant trace of impurity other than Ce.
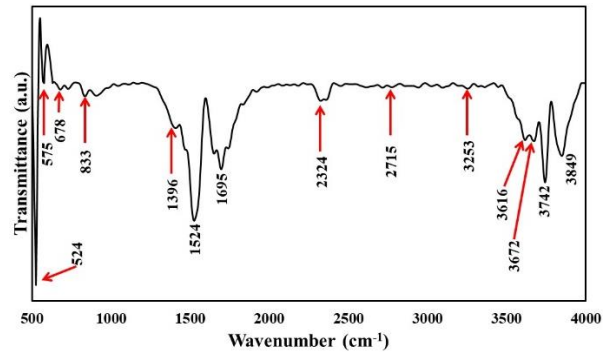
Fig. 3 – FTIR patterns of Ce doped ZnO NPs

3.3 UV-Vis Spectra and Optical Band Gap Study

UV-Vis spectra of CZO nanoparticles were recorded in the wavelength range 200-600 nm at room temperature in transmission mode. The variation is shown in Fig. 4. The CZO sample is highly transparent in nature
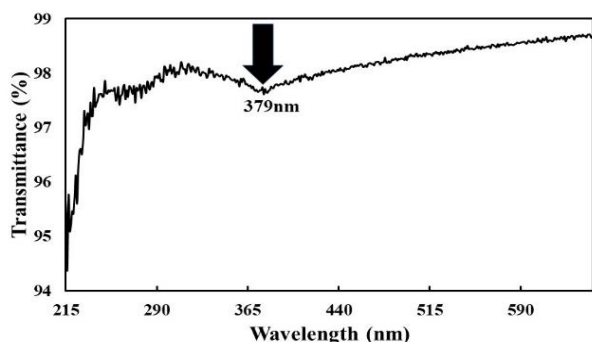
Fig. 4 – UV-Vis spectra of Ce doped ZnO NPs

in the visible region and indicates an absorption dip at 379 nm. The band gap energy (ε_g) of NPs was calculated using the formula:

$$\in_g = \frac{hc}{\lambda}, \qquad (7)$$

where *h* and *c* are Planck's constant and speed of light in vacuum, respectively. The calculated band gap energy for our CZO sample is 3.270 eV. As expected, it clearly shows a red shift of band gap when compared with an undoped ZnO NPs (3.294 eV [5]) prepared and measured under same condition. The shift of absorption dip towards the longer wavelength region is due to the doping of rare earth element (Ce) which forms oxygen vacancies and additional energy levels. Ivetíc et al. [16] noticed a similar kind of behavior for Eu doped ZnO nanostructures. Such red shift may be related to the formation of some shallow level inside the band gap, due to the introduction of impurity atoms (Ce^{3+}) into the ZnO wurtzite lattices structure [13]. In connection to the discussion made by Bomila et al. [13], here it is justified to say that the narrowing of band gap energy due to Ce insertion, is a result of the formation of Ce related, localized, density of states closer to the conduction band minima of ZnO. The existence and connection to the band gap reduction with the formation of such localized electronic states have also been reported and discussed by Kumar et al. [17].

3.4 Photoluminescence (PL) Study

PL spectra (Fig. 5) of the sample was recorded by exciting it with two different excitation wavelengths 310 nm and 325 nm at room temperature. The spectra (Fig. 5) show a broad peak around 380 nm. It is well-known in literature that an intense UV peak centered around 382 nm is identified as near band edge (NBE) emission is an intrinsic property of the wurtzite ZnO and originates from the excitonic recombination process [18]. Again, in our CZO sample, the absence of a PL emission in the visible range is also considered as a signature of high crystalline sample [18].

3.5 Micro-structural Study with FESEM

The surface morphology of CZO NPs is observed by FESEM as represented in Fig. 6 which shows the formation of clusters of CZO NPs with size and morphology. Fig. 6a clearly shows the formation of particle like structure. To understand the mechanism in better way,

we captured higher resolution FESEM photographs which clearly indicates the formation of distorted flower petal like self-assembled structures in our CZO sample. The distortion may be due to a heavy Ce doping. To confirm the presence of Ce, we performed EDX study which is shown in Fig. 7 with the elements present in the sample in a tabular form.
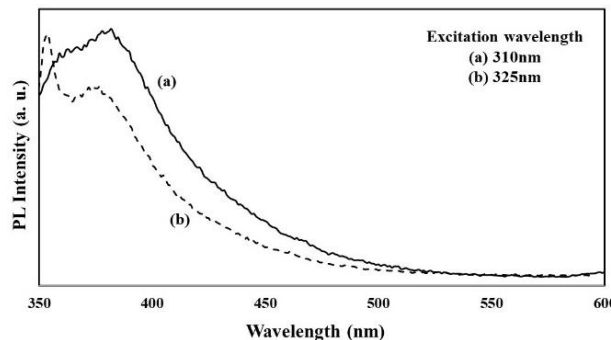

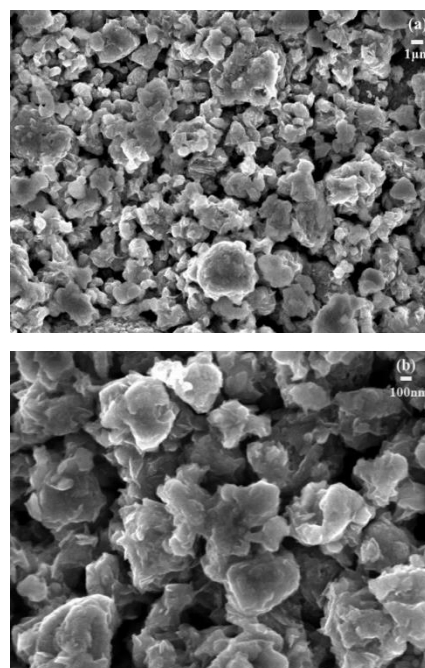**Fig. 5** – Photoluminescence spectrum of Ce doped ZnO NPs

Fig. 6 – FESEM patterns of 10 at. % Ce doped ZnO NPs

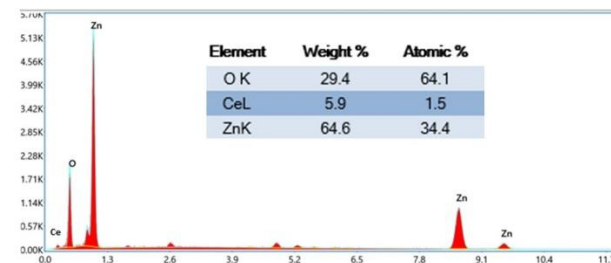| Element	Weight %	Atomic %
O K	29.4	64.1
CeL	5.9	1.5
ZnK	64.6	34.4

Fig. 7 – EDX of Ce doped ZnO NPs

4. CONCLUSIONS

The work explains a simple, low-cost sol-gel method to synthesize ZnO nanoparticles with heavy Ce doping. Prepared sample shows a XRD peak shift towards lower Bragg's angle as compared to undoped sample. It

also indicates a lattice distortion due to doping. Small amount of impurity phases in terms of CeO_2 and Ce_2O_3 are present in prepared samples which is a known fact that only limited Ce^{3+} ions are soluble in the host ZnO matrix. FTIR analysis shows the presence of all desired Zn–O and Ce–O bonds. Band gap analysis shows its lowering due to doping as compared to undoped ZnO. It is because of the defect's states generated during the settlement of dopant in the ZnO host matrix. As the doped Ce particles have larger ionic radius so the possibility of generation of such defect states is obvious and acceptable. PL emission spectra at two different excitation wavelengths shows an intense UV peak centered around 382 nm and is identified as NBE emission, a well-known characteristic of a wurtzite ZnO structure. The FESEM micrographs have distorted flower petal like nanostructures. The distortion is caused by heavy Ce doping. The presence of Ce in the sample is confirmed by EDX spectra. Overall, the work provides an insight to the features of Ce doped ZnO NPs which can be useful to design optoelectronic devices with tunable band gap.

REFERENCES

1. J. Theerthagiri, S. Salla, R.A. Senthil, P. Nithyadharseni, A. Madankumar, P. Arunachalam, T Maiyalagan, H-S Kim, *Nanotechnology* **30**, 392001 (2019).
2. Ü. Özgür, Ya. I. Alivov, C. Liu, A. Teke, M.A. Reshchikov, S. Doğan, V. Avrutin, S.J. Cho, H. Morkoç, *J. Appl. Phys.* **98**, 041301 (2005).
3. K.P. Misra, R.K. Shukla, A. Srivastava, A. Srivastava, *Appl. Phys. Lett.* **95** No 3, 031901 (2009).
4. S. Chattopadhyay, K.P. Misra, A. Agarwala, A. Rao, P.D. Babu, *Mater. Chem. Phys.* **227**, 236 (2019).
5. K.P. Misra, S. Jain, A. Agarwala, N. Halder, S. Chattopadhyay, *Semiconductors* **54** No 3, 311 (2020).
6. P. Das Gupta, S. Chattopadhyay, R.J. Choudhary, D.M. Phase, P. Sen, *Mater. Lett.* **65** No 13, 2073 (2011).
7. R. Röder, S. Geburt, M. Zapf, D. Franke, M. Lorke, T. Frauenheim, A.L. da Rosa, C. Ronning, *Phys. Status Solidi B* **256**, 1800604 (2019).
8. A.L. He, X.Q. Wang, R.Q. Wu, Y.H. Lu, Y.P. Feng, *J. Phys.: Condens. Matt.* **22** No 17, 175501 (2010).
9. T.M. Schmidt, R.H. Miwa, A. Fazzio, *Phys. Rev. B: Condens. Matter.* **81** No 19, 195413 (2010).
10. F.-B. Zheng, C.-W. Zhang, P.-J. Wang, H.-X. Luan, *Solid State Commun.* **152** No 14, 1199 (2012).
11. C. Tan, D. Xu, K. Zhang, X. Tian, W. Cai, *J. Nanomater.* **215**, 329570 (2015).
12. C. Jayachandraiah, G. Krishnaiah, *J. Mater Sci.* **52**, 7058 (2017).
13. R. Bomila, S. Srinivasan, A. Venkatesan, B. Bharath, K. Perinbam, *Mater. Res. Innovations* **22** No 7, 379 (2017).
14. S. Chattopadhyay, K.P. Misra, A. Agarwala, A. Shahee, S. Jain, N. Halder, A. Rao, P.D. Babu, M. Saran, A.K. Mukhopadhyay, *Ceram Int.* **45**, 23341 (2019).
15. Md. Elias, Md.K. Amin, S.H. Firoz, Md.A. Hossain, S. Akter, Md.A. Hossain, Md.N. Uddin, I.A. Siddiquey, *Ceram. Int.* **43**, 84 (2017).
16. T.B. Ivetić, M.R. Dimitrievska, I.O. Gˊuth, Lj.R. Dačanin, S.R. Lukićʹ-Petrovićʹc, *J. Res. Phys.* **36** No 1, 43 (2012)
17. D.R. Kumar, K.S. Ranjith, R.T.R. Kumar, *Optik* **154**, 115 (2018).
18. J.L. Cervantes-López, R. Rangel, J. Espino, E. Martínez, R. García-Gutiérrez, P. Bartolo-Pérez, J.J. Alvarado-Gil, O.E. Contreras, *Appl. Phys. A* **123**, 86 (2017).

Зменшення забороненої зони та утворення пелюсткової наноструктури в нанопорошках ZnO, сильно легованих Ce

Kamakhya Prakash Misra[1], Ashok Kumawat[1], Priyanka Kumari[2], Susruta Samanta[2], Nilanjan Halder[1], Saikat Chattopadhyay[1]

[1] *Department of Physics, School of Basic Sciences, Manipal University Jaipur, Jaipur, Rajasthan 303007, India*
[2] *Department of Chemistry, School of Basic Sciences, Manipal University Jaipur, Jaipur, Rajasthan 303007, India*

Метою дослідження є вивчення структурної та оптичної поведінки системи наночастинок ZnO, сильно легованих Ce. Для синтезу наночастинок застосовано добре відомий хімічний метод золь-гелю та охарактеризовано їх структурні, оптичні та морфологічні особливості. Рентгенографічний аналіз (XRD) та енергодисперсійна рентгенівська спектроскопія (EDX) підтверджують наявність атома Ce у підготовленому зразку. Дані XRD підтверджують, що іони Ce^{3+} займають місця іонів Zn^{2+} у гексагональній решітці ZnO під час легування. Завдяки більш високій концентрації легування надлишок Ce показує присутність змішаних фаз CeO_2 та Ce_2O_3 у зразку. Аналіз Вільямсона-Хола допомагає отримати профіль мікродеформації у вирощеному зразку. Дослідження UV-Vis підтверджує зміщення забороненої зони в легованих зразках, а дослідження фотолюмінесценції вказує на наявність дефектних станів, які є причиною переходів поблизу країв зони у зразках. Підготовлені зразки також характеризували за допомогою FESEM для аналізу морфології поверхні та нанокристалічних структур.

Ключові слова: ZnO, Рідкоземельний матеріал, Легування, Наночастинки, Заборонена зона, Фотолюмінесценція.